

Theoretical study of effects of the entrance channel on the relative yield of complete fusion and quasifission in heavy-ion collisions within a dinuclear system approach

S. Soheyli* and M. Varasteh Khanlari

Department of Physics, Bu-Ali Sina University, Post Code 6517433391, Hamedan, Iran

(Received 10 July 2016; published 22 September 2016)

The relative yield of complete fusion and quasifission components for the $^{12}\text{C} + ^{204}\text{Pb}$, $^{19}\text{F} + ^{197}\text{Au}$, $^{30}\text{Si} + ^{186}\text{W}$, and $^{48}\text{Ca} + ^{168}\text{Er}$ reactions which all lead to the compound nucleus ^{216}Ra are analyzed to calculate the entrance channel effects by comparison of capture, complete fusion, and quasifission cross sections, emission barriers (B_{fus}^* , B_{qf}^*), as well as complete fusion probability estimated by statistical method within the framework of the dinuclear system model. The difference among complete fusion probabilities calculated by the dinuclear system model for different entrance channels can be explained by the hindrance to complete fusion due to the larger inner fusion barrier B_{fus}^* for the transformation of the dinuclear system into a compound nucleus and the increase of the quasifission contribution due to the decreasing of the emission barrier B_{qf}^* of quasifission as a function of the angular momentum. Although these reactions with different entrance channels populate the same compound nucleus ^{216}Ra at similar excitation energies, the model predicts the negligible quasifission probability for reactions having higher entrance channel mass asymmetry and the dominant decay channel is complete fission. For reactions induced by massive projectiles such as Si and Ca having lower entrance channel mass asymmetry, the quasifission component is dominant in the evolution of dinuclear system, and the fusion process is extremely hindered.

DOI: [10.1103/PhysRevC.94.034615](https://doi.org/10.1103/PhysRevC.94.034615)

I. INTRODUCTION

The collision of two massive nuclei leads to a variety of nuclear processes such as deep inelastic, complete fusion, quasifission, fast fission, fusion-fission, and evaporation of particles. The major stage of all channels includes the formation of the excited and rotating dinuclear system. The evolution of two heavy colliding ions is usually divided into three stages. The first step is the capture mechanism of the projectile nucleus by the target nucleus to overcome the entrance barrier. The second step is clustering or the formation of an asymmetric dinuclear system (DNS) in the excited state with the relative motion of the colliding nuclei in the interaction potential, so that the beam energy and orbital angular momentum ℓ of the relative motion of nuclei to be converted in the excitation energy and orbital angular momentum of the DNS. The last step consists of the binary decay of the DNS called quasifission process to pass over the quasifission barrier on the radial distance. The other way replaced, the transfer of nucleons in the mass asymmetry degree of freedom $\eta = \frac{|(A_1 - A_2)|}{A}$ (where A_1 and A_2 are the mass numbers of nuclei and $A = A_1 + A_2$) between two nuclei and the formation of the compound nucleus (complete fusion) by overcoming the inner fusion barrier B_{fus}^* . After the formation of DNS, there is a very strong competition between the quasifission and the complete fusion processes which decreases the probability of the compound nucleus formation. It is now understood that the dominant mechanism has a strong dependence on entrance channel properties such as mass asymmetry [1–3], beam energy [4,5], and orientation angle between the eventual symmetry axes of colliding nuclei [6,7], as well as on the fissility [8,9] of the compound nucleus being formed. It has also been

shown to be sensitive to nuclear structure effects such as static deformation [4,5], closed shells [10,11]. The understanding of the complete fusion of two massive nuclei implies a detailed investigation of the decay products of the compound nucleus, of the fragments of quasifission and fast fission processes which compete with the complete fusion mechanism [12]. The complete fusion takes place during the descent of the dinuclear system from the Businaro-Gallone (BG) point. The BG point, in other words the smallest value of excitation energy of dinuclear system, is determined by the top value of the driving potential. This point corresponds to the saddle point on the way to complete fusion [13,14]. The quasifission process is considered as an intermediate process between a deep inelastic process and the formation of an equilibrated compound nucleus through complete fusion. Therefore, at the quasifission process, the dinuclear system never becomes as compact as the compound nucleus. A strong quasifission component is observed in the reaction between spherical nuclei, as well as in the reaction induced by the spherical projectile over deformed target. The quasifission products lead to anisotropy angular distributions. Angular anisotropy of the fusion-fission and quasifission fragments for reactions with massive nuclei are estimated in the framework of the DNS model in Refs. [7,15]. The effects of deformation and orientation of the interacting nuclei contributing to the nuclear and Coulomb interactions of the DNS model are studied in Refs. [16,17]. The authors demonstrated that the two nuclei become more compact with a belly-belly orientation in contrast to the pole-pole one, in other words the minimum of the potential energy for a belly-belly orientation is at a smaller distance than that of the pole-pole case. They also found that the potential energy is sensitive to the considered orientation of colliding nuclei. The role of the orientation angles of the symmetry axes of the deformed projectile and target nucleus relative to the beam direction in the fusion and capture

*Corresponding author: s.soheyli@basu.ac.ir

processes in heavy-ion collisions has also been studied [18]. Fast fission is a binary decay which takes place only at high values of angular momentum $\ell > \ell_f$, where ℓ_f is a value of ℓ at which the fission barrier of the considering nucleus disappears. Therefore, one can say that the role of fast fission becomes important only at higher energies. Here, we use the DNS model as detailed earlier for the deep inelastic reaction and applied for the quasifission process. The major advantage of this model over other models is that it takes into account the competition between complete fusion and quasifission processes in the DNS. This model supplies good agreement between the theoretical predictions and experimental data for the fusion of heavy ions. Therefore, the DNS model was successfully applied to the description of heavy-ion fusion reactions. In the present paper, the internuclear potential energy, emission barriers for binary decay, complete fusion probability, and excitation functions of capture, fusion, and quasifission processes, as well as the relative yield of complete fusion and quasifission components have been estimated for the $^{12}\text{C} + ^{204}\text{Pb}$, $^{19}\text{F} + ^{197}\text{Au}$, $^{30}\text{Si} + ^{186}\text{W}$, and $^{48}\text{Ca} + ^{168}\text{Er}$ reactions leading to the same compound nuclei ^{216}Ra , but having different mass asymmetric in the entrance channel within the framework of the combined dynamical model base on the conception of the dinuclear system. The calculations connected with the mentioned reactions are performed for the first time in the DNS model. The study of these reactions with different mass asymmetry parameters can be useful to investigate the role of the entrance channel in the formation of the complete fusion and quasifission products.

The paper is organized in the following way. The description of theoretical approach is given in Sec. II. Section III is devoted to our calculations and our results. Section IV contains the conclusions of this investigation.

II. OUTLINE OF THEORETICAL APPROACH

The configuration of clustering is a nuclear molecule or a dinuclear system (DNS) formed after the capture mechanism of the projectile nucleus by the target nucleus. The DNS consists of two nuclei which touch each other and keep their own individuality [19]. One of the main freedom degrees of the dinuclear model is the exchange of nucleons between clusters that change the mass and charge asymmetries. The transfer of nucleons between the clusters of the DNS is explained by the numerical solution of the master equation.

The dinuclear system formed after capture mechanism evolves to complete fusion by increasing its mass asymmetry. A path to complete fusion is determined by the internuclear potential energy surface (PES); $U(A, Z; R)$. Assuming a small overlap of nuclei in the DNS, $U(A, Z; R)$ is calculated versus charges Z_1, Z_2 ($Z_2 = Z_{\text{CN}} - Z_1$) forming the dinuclear system and the distance R between their centers [18]

$$U(A, Z; R) = Q - V_{\text{rot}}^{\text{CN}}(\ell) + V(R, Z_1, Z_{\text{CN}} - Z_1, \ell, \beta_i), \quad (1)$$

$$Q = B_1(Z_1) + B_2(Z_{\text{CN}} - Z_1) - B_{\text{CN}}(Z_{\text{CN}}), \quad (2)$$

where B_1, B_2 , and $B_{\text{CN}}(Z_{\text{CN}})$ are the binding energies of the fragments in the DNS at their ground states and of the compound nucleus, respectively, which are taken from [20]. $\beta_i (i =$

1, 2) are the quadrupole deformation parameters obtained from the tables of Ref. [21]. The rotational energy $V_{\text{rot}}^{\text{CN}}(\ell)$ of the compound nucleus (CN) is defined as $V_{\text{rot}}^{\text{CN}}(\ell) = \frac{(\hbar^2 \ell(\ell+1))}{2\mathfrak{I}_{\text{CN}}}$, where \mathfrak{I}_{CN} is the rigid-body moment of inertia of the CN.

The nucleus-nucleus interaction potential $V(R, Z_1, Z_{\text{CN}} - Z_1, \ell, \{\beta_i\})$ holding the DNS for the given charge and mass asymmetry includes Coulomb (V_C), nuclear (V_N), and rotational ($V_{\text{rot}}^{\text{DNS}}$) potentials,

$$\begin{aligned} V(R, Z_1, Z_{\text{CN}} - Z_1, \ell, \{\beta_i\}) \\ = V_C(R, Z_1, Z_{\text{CN}} - Z_1, \{\beta_i\}) + V_N(R, Z_1, Z_{\text{CN}} - Z_1, \{\beta_i\}) \\ + V_{\text{rot}}^{\text{DNS}}(\ell, \{\beta_i\}). \end{aligned} \quad (3)$$

The shapes of nuclei are most important in the calculation of Coulomb and nuclear interaction potentials between the colliding nuclei. The Coulomb potential is taken from Ref. [22] as follows:

$$\begin{aligned} V_C(R, Z_1, Z_2, \{\beta_i\}) \\ = \frac{Z_1 Z_2}{R} e^2 + \frac{Z_1 Z_2}{R^3} e^2 \left\{ \left(\frac{9}{20\pi} \right)^{1/2} \sum_{i=1}^2 R_i^2 \beta_i P_2(\cos \alpha_i) \right. \\ \left. + \frac{3}{7\pi} \sum_{i=1}^2 R_i^2 [\beta_i P_2(\cos \alpha_i)]^2 \right\}, \end{aligned} \quad (4)$$

where α_1 and α_2 are the angles between symmetry axes of statically deformed nuclei and radius vectors, $R_i = 1.16A_i^{1/3}$. For the nuclear part of potential V_N , we use a double folding formalism with the effective density-dependent nucleon-nucleon interaction [23], which is known from the theory of finite Fermi systems. As a result of various calculations, the following simple approximate expression is obtained for deformed nuclei in the pole-pole orientation [24]:

$$\begin{aligned} V_N(R, Z_1, Z_{\text{CN}} - Z_1, \{\beta_i\}) \\ = V_0 \left\{ \exp \left[-2 \frac{(R - R_{12})\alpha}{R_{12}} \right] - 2 \exp \left[- \frac{(R - R_{12})\alpha}{R_{12}} \right] \right\}. \end{aligned} \quad (5)$$

Here V_0 is the strength of the potential and this quantity is given by

$$\begin{aligned} V_0 = 2\pi a_1 a_2 \bar{R} (11.3 - 0.82 \bar{R}_0) \\ \times \left(1 + \frac{0.16 (\sum_{i=1}^2 \beta_i)}{(1 + \exp[-17(|\eta| - 0.5)])} \right), \end{aligned} \quad (6)$$

where $a_1 = 0.56$ fm and $a_2 = a_1 - 0.015|\eta|$ are the surface diffuseness parameters of the heavy and light nuclei in the DNS (the light nucleus has small diffuseness), and $\eta = \frac{(A_1 - A_2)}{(A_1 + A_2)}$ is a mass asymmetry collective coordinate as mentioned before. The quantities \bar{R}_0 and \bar{R} in the above equation are defined by the following equations:

$$\bar{R}_0 = \frac{R_1 R_2}{(R_1 + R_2)}, \quad (7)$$

$$\bar{R} = \frac{R_1 R_2}{(R_1 + R_2)}. \quad (8)$$

The quantity $\overline{R}_i (i = 1, 2)$ is also given by

$$\overline{R}_i = D_i \frac{1 + (5/4\pi)^{1/2} \beta_i - 1/4\pi \beta_i^2}{1 + 4(\frac{5}{4\pi})^{1/2} \beta_i - \frac{1}{4\pi} \beta_i^2}. \quad (9)$$

Here, $D_i (i = 1, 2) = R_i [1 + (\frac{5}{4\pi})^{1/2} \beta_i - \frac{1}{4\pi} \beta_i^2]$. R_{12} and α in Eq. (5) are also determined by the following equations, respectively:

$$R_{12} = D_1 + D_2 + 0.1 \text{ fm}, \quad (10)$$

$$\alpha = (11.47 - 17.32a_1a_2 + 2.07\overline{R}_0)[1 + 0.25(\sum_{i=1}^2 \beta_i)]. \quad (11)$$

The rotational energy of the DNS is also defined as [24]

$$V_{\text{rot}}^{(\text{DNS})}(R, \ell, \{\beta_i\}) = \frac{\hbar^2 \ell(\ell + 1)}{2\mathfrak{I}_{\text{DNS}}(R, A, \{\beta_i\})}. \quad (12)$$

The moments of inertia $\mathfrak{I}_{\text{DNS}}$ of the formed DNS is calculated as

$$\mathfrak{I}_{\text{DNS}}(R, A, \{\beta_i\}) = \mathfrak{I}_1 + \mathfrak{I}_2 + \mu R^2, \quad (13)$$

where $\mathfrak{I}_i (i = 1, 2)$ are the moments of inertia of the DNS nuclei obtained in the rigid-body approximation as [25]

$$\mathfrak{I}_i = \frac{1}{5} m_o A_i (a_i^2 + b_i^2), \quad (14)$$

$$a_i = R_i \left(1 - \frac{\beta_i^2}{4\pi}\right) \left(1 + \sqrt{\frac{5}{4\pi}} \beta_i\right),$$

$$b_i = R_i \left(1 - \frac{\beta_i^2}{4\pi}\right) \left(1 - \sqrt{\frac{5}{16\pi}} \beta_i\right). \quad (15)$$

Here, m_o is the mass of a nucleon. When the nucleus-nucleus potential is calculated at the capture stage, the value of $\mathfrak{I}_{\text{DNS}}(R, A, \{\beta_i\})$ is replaced by μR^2 .

The ratios $\frac{A_1}{Z_1}$ and $\frac{A_2}{Z_2}$ for both fragments (or the distribution of neutrons between two fragments with the given proton numbers Z_1 and Z_2) were determined by minimizing $U(A_1, Z_1, R)$ with respect to the mass asymmetry A_1 for each charge asymmetry Z_1 [18].

The DNS model is also used for the analysis of the competition between complete fusion and quasifission in almost symmetric massive DNSs. This competition may reduce greatly the fusion cross section with a reduction in the asymmetry in the entrance channel. According to the statistical approaches, the probability of complete fusion is connected to the ratio of the level densities and depends on the inner fusion or quasifission barriers. The fusion probability of the DNS or hindrance factor to complete fusion P_{CN}^Z as a function of E_{DNS}^* is given by the following expression [26]:

$$P_{\text{CN}}^Z(E_{\text{DNS}}^*) = \frac{\rho(E_{\text{DNS}}^* - B_{\text{fus}}^*)}{\rho(E_{\text{DNS}}^* - B_{\text{fus}}^*) + \rho(E_{\text{DNS}}^* - B_{qf})}, \quad (16)$$

where $\rho(E_{\text{DNS}}^* - B_k^*)$ is the level density for the DNS at the quasifission and inner fusion barriers ($B_k^* = B_{qf}, B_{\text{fus}}^*$). The local excitation energy E_{DNS}^* of each DNS is factorized as follows [25]:

$$E_{\text{DNS}}^* = E_{\text{CN}}^*(\ell) - U(R_m, Z, A, \ell), \quad (17)$$

where $E_{\text{CN}}^*(\ell) = E_{\text{c.m.}} + Q - V_{\text{rot}}^{\text{CN}}(\ell)$ is the excitation energy of the compound nucleus formed in the reaction. The barrier B_{qf} in the DNS approach is defined as

$$B_{qf}(Z, A, \ell) = V(R_b, Z, A, \beta_1, \beta_2, \ell) - V(R_m, Z, A, \beta_1, \beta_2, \ell). \quad (18)$$

The R_m is the minimum of the nucleus-nucleus potential well which is called the pocket potential. The situation of this pocket for the pole-pole orientation is the distance between the nuclei $R_m \approx R_1[1 + \sqrt{\frac{5}{4\pi}} \beta_1] + R_2[1 + \sqrt{\frac{5}{4\pi}} \beta_2] + 0.5 \text{ fm}$ corresponding to the touching configuration with a possible deformation of the heavy cluster. The $R_b \approx R_m + 1.5 \text{ fm}$ corresponds to the position of the Coulomb barrier in the DNS under consideration [27].

The inner fusion barrier B_{fus}^* is a dynamical hindrance in the DNS evolution to form the compound nucleus in the mass asymmetry coordination of the DNS system. This barrier in the framework of the DNS model is defined as the difference of the driving potential at the BG point and its value at the injection point of the considered reaction [28]

$$B_{\text{fus}}^*(Z_P, A_P, \ell) = U_{\text{max}}(Z_{\text{max}}, A_{\text{max}}, R_m(Z_{\text{max}}, A_{\text{max}}), \ell) - U_{\text{in}}(Z_P, A_P, R_m(Z_P, A_P), \ell), \quad (19)$$

where Z_{max} and A_{max} are the charge and the mass number of a fragment of DNS corresponding to the maximum value of driving potential, Z_P and A_P are the charge and the mass number of the projectile, respectively.

The level density of the DNS is factorized as follows [14]:

$$\begin{aligned} \rho(E_{\text{DNS}}^* - B_k^*) &= \left[\frac{g^2(E_f)}{g_1(E_f)g_2(E_f)} \right]^{1/2} \exp \left[2\pi \left(\frac{g(E_f)(E_{\text{DNS}}^* - B_k^*)}{6} \right)^{1/2} \right] \\ &\times \frac{1}{2\sqrt{48} \left[\frac{3}{2} g(E_f)(E_{\text{DNS}}^* - B_k^*) \right]^{1/4} (E_{\text{DNS}}^* - B_k^*)}, \quad (20) \end{aligned}$$

where $g_i = A_i E_f^{-1}$ are densities of single-particle levels of the DNS fragments near the Fermi surface for the DNS nuclei; $g = \frac{g_1 + g_2}{2}$ and the Fermi level energy E_f is equal to 37 MeV. The fusion probability $P_{\text{CN}}(E_{\text{DNS}}^*, \ell)$ of the DNS is calculated according to the following formula [18]:

$$P_{\text{CN}}(E_{\text{DNS}}^*, \ell) = \sum_{Z_{\text{sym}}}^{Z_{\text{max}}} Y_Z(E_{\text{DNS}}^*) P_{\text{CN}}^{(Z)}(E_{\text{DNS}}^*, \ell). \quad (21)$$

Here, $Z_{\text{sym}} = \frac{(Z_1 + Z_2)}{2}$ and Z_{max} corresponds to the point where the driving potential reaches its maximum [$B_{\text{fus}}^*(Z_{\text{max}}) = 0$] [29–31]. $Y_Z(E_{\text{DNS}}^*)$ is the probability of population of the configuration ($Z_1, Z_2 = Z_{\text{CN}} - Z_1$) at E_{DNS}^* and ℓ .

The partial capture cross section is determined by the capture probability $\wp_{\text{cap}}^\ell(E_{\text{c.m.}})$ which means that the colliding nuclei are trapped into the pocket of the nucleus-nucleus potential, appeared as the result of the competition between the long-range repulsive Coulomb interaction and the short-range attractive nuclear forces. The capture cross section can be written as [18]

$$\sigma_{\text{cap}}(E_{\text{c.m.}}) = \frac{\pi \hbar^2}{2\mu E_{\text{c.m.}}} \sum_{\ell_{\text{min}}}^{\ell_{\text{max}}} \ell(\ell + 1) \wp_{\text{cap}}^\ell(E_{\text{c.m.}}). \quad (22)$$

Here, μ is the reduced mass of the system, $E_{c.m.}$ is the energy of the system in center-of-mass frame, $\wp_{cap}^\ell(E_{c.m.})$ is the transmission probability which depends on the collision dynamics and is determined by the Hill-Wheeler formula [25]

$$\wp_{cap}^\ell(E_{c.m.}) = \left\{ 1 + \exp \left[2\pi \frac{(V(R_b, A_i, \beta_i = 0, \ell) - E_{c.m.})}{\hbar\omega_\ell} \right] \right\}^{-1}, \quad (23)$$

where the effective potential of two nuclei for the given DNS configuration is approximated near the Coulomb barrier placed at R_b by the inverted harmonic oscillator potential with the barrier height $V(R_b, A_i, \ell)$ and the frequency $\omega(\ell)$.

When the beam energy is much larger than the Coulomb barrier, ℓ_{min} can be nonzero. The maximum value of angular momentum ℓ leading to capture ℓ_{max} depends on the beam energy and it is determined by set as $\ell_{max} = \min\{\ell_{kin}, \ell_{cr}\}$, where the kinematical angular momentum is defined as $\ell_{kin} = \{2\mu[E_{c.m.} - V(R_b, Z_i, A_i, \beta_i = 0, \ell = 0)]\}^{1/2} \frac{R_b}{\hbar}$ [25]. The critical value of angular momentum ℓ_{cr} for a given beam energy can be calculated according to the following expression:

$$\ell_{cr} \approx R_F \sqrt{\frac{2\mu}{\hbar^2} (E_{c.m.} - V_F)}, \quad (24)$$

where the fusion radius R_F is given by

$$R_F = r_o (A_1^{1/3} + A_2^{1/3}) + d, \quad (25)$$

where d is the distance of the sharp nuclear surfaces at the fusion barrier. The fusion barrier V_F is equal to the height of the potential barrier $V(R_F)$ for head-on collisions and the fusion radius R_F is the corresponding radial distance

$$\left. \frac{dV(R)}{dR} \right|_{R=R_F} = 0. \quad (26)$$

In this relation, $V(R)$ is the sum of the Coulomb V_C and the nuclear V_N potentials; $V(R) = V_N(R) + V_C(R)$. The potential V_F can be interpreted as the fusion barrier

$$V_F = \frac{Z_1 Z_2 e^2}{r_o (A_1^{1/3} + A_2^{1/3}) + a + d}, \quad (27)$$

where $a = 1.4$ fm is the nuclear force range parameter [32].

At the value $\ell = \ell_{max}$, the potential pocket disappears in the entrance channel. Therefore, the capture mechanism of the projectile and the target is impossible at angular momenta larger than ℓ_{max} .

The partial cross section of the complete fusion is determined by the product of the partial capture cross section and the probability P_{CN} of the compound nucleus formation taking into account the competition between complete fusion and quasifission channels [18]:

$$\sigma_{fus}(E) = \sum_{\ell_{min}=0}^{\ell_{max}} \sigma_{cap}^\ell(E) P_{CN}(\ell). \quad (28)$$

According to the DNS approach, quasifission cross section is extracted by the following relation [18]:

$$\sigma_{qf}(E) = \sum_{\ell_{min}=0}^{\ell_{max}} \sigma_{cap}^\ell(E) (1 - P_{CN}(\ell)), \quad (29)$$

where it depends on the partial capture cross section for the transition of the colliding nuclei over the entrance Coulomb

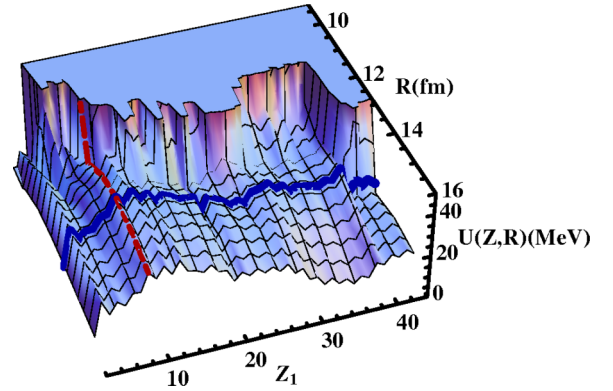


FIG. 1. The potential energy surface calculated for the DNS formed in the reactions leading to the formation of the same compound nucleus ^{216}Ra as a function of the relative distance R between colliding nuclei and the charge number Z_1 of one of the DNS fragments based on the DNS approach. The blue broken line corresponds to the driving potential $U(R_m)$ which is determined by the minimum values of the potential wells for each charge value Z_1 . The red dashed curve corresponds to the nucleus-nucleus interaction potential $V(R)$ which is determined by a given charge Z_1 for each value R .

barrier and on the probability P_{CN} of the compound nucleus formation after the capture.

III. RESULT AND DISCUSSION

The theoretical analysis of the $^{12}\text{C} + ^{204}\text{Pb}$, $^{19}\text{F} + ^{197}\text{Au}$, $^{30}\text{Si} + ^{186}\text{W}$, and $^{48}\text{Ca} + ^{168}\text{Er}$ reactions leading to the same compound nuclei ^{216}Ra is the subject of discussion in the present paper. In the DNS approach, the potential energy has an important role and depends on the masses of the products in the quasifission process. The potential energy surface of the DNS corresponding to the compound nucleus of ^{216}Ra calculated according to Eq. (1) as a function of the relative distance R of DNS nuclei and charge asymmetry Z_1 (the charge of one of the fragments) is presented in Fig. 1. The blue broken line indicates the driving potential $U(R_m)$ which is estimated by the minimum values of the potential pockets for each charge value Z_1 . The red dashed curve presents the interaction potential $V(R)$ of two nuclei in DNS which is estimated by a given charge Z_1 for each value R .

The driving potential $U(R_m)$ is extracted from the potential energy surface $U(A, Z; R)$, where R_m is the internuclear distance corresponding to the minimum of their nucleus-nucleus potential $V(R)$. The calculation of the driving potential $U(R_m)$ is done for different entrance channels which could lead to the formation of the same compound nucleus ^{216}Ra . In Fig. 2, the curves are $U(R_m)$ as a function of the charge Z_1 of the lighter fragment of the DNS at the different values of the orbital angular momentum ℓ . The blue dashed, green dot-dashed, and red solid curves (curves from top to bottom) correspond to the driving potential at $\ell = 0, 30$, and $50 \hbar$, respectively.

Our calculations indicate that the values of $U(R_m)$ for each Z_1 reduce with increasing orbital angular momentum ℓ , as well

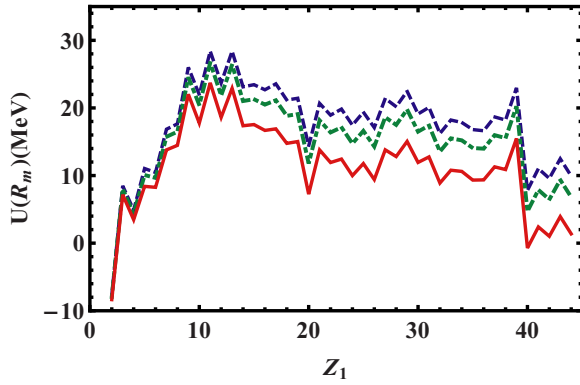


FIG. 2. The driving potential calculated for the DNS formed in the reactions leading to the formation of the same compound nucleus ^{216}Ra as a function of the charge of the DNS fragment Z_1 for the different values of angular momentum ℓ based on the DNS approach. The blue dashed, green dot-dashed, and red solid curves (curves from top to bottom) correspond to the driving potential of the products at $\ell = 0, 30$, and $50 \hbar$, respectively.

as disclose dependence of value of $U(R_m)$ on mass asymmetry of DNS fragments.

The cut of the potential energy surface for a given charge Z is the nucleus-nucleus interaction potential $V(R)$. In Fig. 3, we present the curves related to $V(R)$ against the distance R between centers of DNS fragments for the four entrance channels which will lead to the same compound nucleus ^{216}Ra

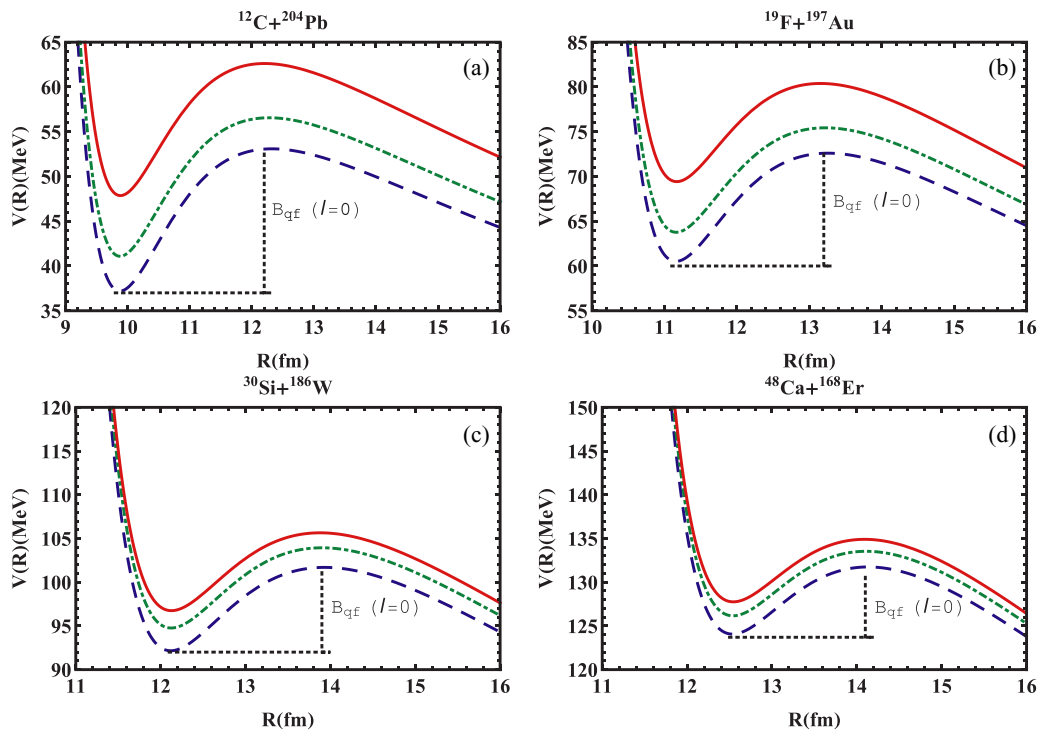


FIG. 3. The nucleus-nucleus interaction potential wells $V(R)$ for the DNS formed in the four reactions namely (a) $^{12}\text{C} + ^{204}\text{Pb}$, (b) $^{19}\text{F} + ^{197}\text{Au}$, (c) $^{30}\text{Si} + ^{186}\text{W}$, and (d) $^{48}\text{Ca} + ^{168}\text{Er}$, which all lead to the compound nucleus ^{216}Ra as a function of the distance R between centers of DNS fragments for the different values of angular momentum ℓ based on the DNS approach. The blue dashed, green dot-dashed, and red solid curves (curves from bottom to top) correspond to the driving potential of the products at $\ell = 0, 30$, and $50 \hbar$, respectively.

TABLE I. Charge asymmetry, inner fusion B_{fus}^* and quasifission B_{qf} barriers, and fusion factor P_{CN} for the studied reactions leading to the ^{216}Ra .

Reactions	η	B_{fus}^* (MeV)	B_{qf} (MeV)	$P_{\text{CN}} \times 10^2$
$^{12}\text{C} + ^{204}\text{Pb}$	0.89	0.00	13.19	99.80
$^{19}\text{F} + ^{197}\text{Au}$	0.82	0.00	10.41	99.78
$^{30}\text{Si} + ^{186}\text{W}$	0.72	5.27	8.36	85.34
$^{48}\text{Ca} + ^{168}\text{Er}$	0.56	14.02	6.81	2.25

at the different values of ℓ . The blue dashed, green dot-dashed, and red solid curves (curves from bottom to top) correspond to $V(R)$ at $\ell = 0, 30$, and $50 \hbar$, respectively.

It is observed that $V(R)$ increases with increasing the orbital angular momentum ℓ for the studied reactions as shown in Fig. 3. Therefore, the depth B_{qf} of the potential pocket reduces with increasing ℓ due to the growth of the repulsive centrifugal part in Eq. (4). It is seen that the contribution of quasifission component decreases due to the reduction of the quasifission B_{qf} barrier if the mass asymmetry of reactions changes from asymmetric values to symmetric ones. The inner fusion B_{fus}^* and quasifission B_{qf} barriers and fusion factor P_{CN} at $\ell = 0$ for the different four channels leading to the same dinuclear system corresponding to the compound nucleus ^{216}Ra are calculated by using Eqs. (19), (18), (16), and (20), respectively. The obtained results are listed in Table I. In these reactions, Z_{max} is equal to 11.

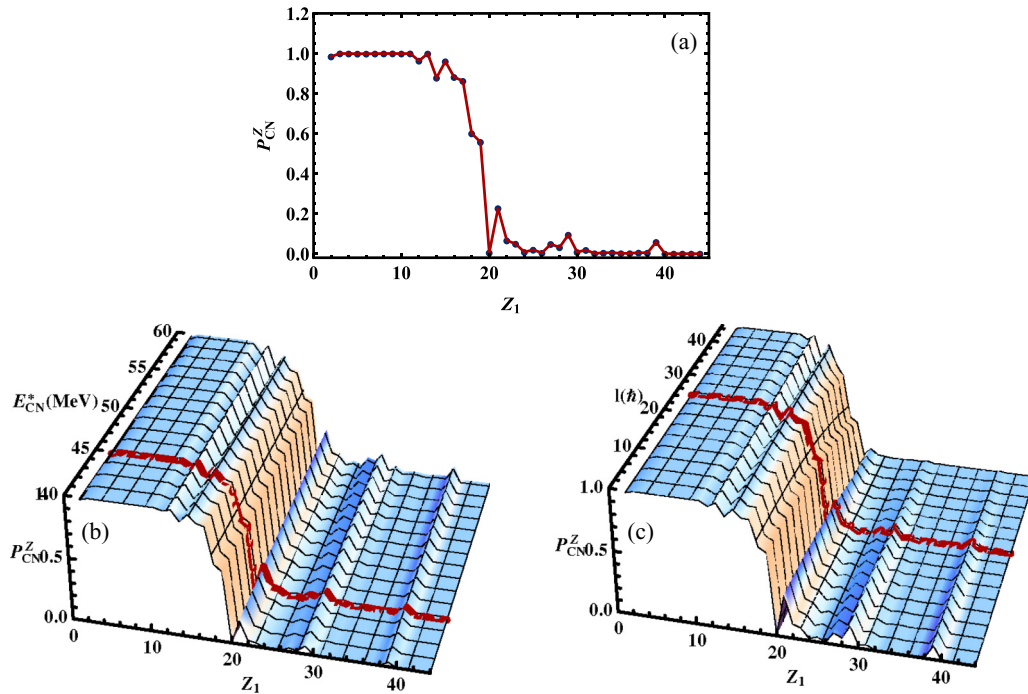


FIG. 4. The calculated probability of complete fusion P_{CN}^Z (dots) for the DNS formed in the reactions leading to the compound nucleus ^{216}Ra as a function of Z_1 at the CN excitation energy $E_{\text{CN}}^* = 45$ MeV, and at $\ell = 25\hbar$ in the framework of the DNS model. (a) Obtained results for P_{CN}^Z in the framework of the DNS model against Z_1 and E_{CN}^* . (b) The complete fusion probability P_{CN}^Z calculated in the DNS model as a function of charge value Z_1 and the angular momentum ℓ . (c) The red solid (dark) lines corresponding to cut of P_{CN}^Z at $E_{\text{CN}}^* = 45$ MeV and at $\ell = 25\hbar$ for each value Z_1 are shown in Figs. 6(a) and 6(b), respectively.

The quasifission B_{qf} barrier is sufficiently large for the reactions having higher mass asymmetry. The values of large quasifission B_{qf} and small intrinsic fusion B_{fus}^* barriers promote the formation of the compound nucleus. The values of these emission barriers depend on the mass asymmetry and orbital angular momentum of the entrance channel.

A. The complete fusion probability for the DNS nuclei

The DNS model was also utilized for determining the complete fusion probability. The value of this probability is very sensitive to the specific form of the driving potential. When the value of the entrance channel mass asymmetry becomes more symmetric, this probability will significantly decrease due to the break up of the DNS before complete fusion. To investigate the dependence of complete fusion probability P_{CN}^Z on the charge (mass) asymmetry of the initial DNS, we performed the calculation of the complete fusion probability P_{CN}^Z for all populated DNS configurations according to Eq. (16). The obtained results based on the DNS approach are presented in Fig. 4. Panel (a) shows the variations of P_{CN}^Z (dots) in terms of the charge number of one of the fragments in DNS for the composite system of ^{216}Ra at the given quantities of $E_{\text{CN}}^* = E_{\text{c.m.}} + Q = 45$ MeV and $\ell = 25\hbar$ as a red solid broken line. It is seen that the P_{CN}^Z values change with increasing charge asymmetry and for the most asymmetry systems are equal to around 1. The dependence of the P_{CN}^Z on the excitation energy E_{CN}^* and the charge value Z_1 , as well as on the angular momentum ℓ and the charge value

Z_1 are represented in panels (b) and (c), respectively. The red broken (dark) lines correspond to the cut of the complete fusion probability P_{CN}^Z at $E_{\text{CN}}^* = 45$ MeV and at $\ell = 25\hbar$ for each charge value Z_1 are shown in Figs. 4(b) and 4(c), respectively.

The dependence of the complete fusion probability P_{CN}^Z (dots) on the quasifission barrier B_{qf} of the initial DNS is plotted for all populated DNS configurations based on the DNS approach in Fig. 5. The variations of P_{CN}^Z in terms of the quasifission B_{qf} barrier for the composite system of ^{216}Ra for the given quantities of $E_{\text{CN}}^* = 45$ MeV and $\ell = 25\hbar$ is shown in panel (a). It is seen that the probability P_{CN}^Z values change with the variation of quasifission barrier B_{qf} of the initial DNS. On the other hand, the probability of the CN formation increases with increasing B_{qf} [$B_{qf} \leq 10$ MeV], and then approximately approaches the constant value 1. Therefore, in the systems with the high asymmetry having the deeper interaction potential pocket, P_{CN}^Z is almost equal to 1. It is already shown that the barrier B_{qf} plays a crucial role in the complete fusion, and depends on the charge asymmetry and angular momentum of the DNS.

The general behavior of P_{CN}^Z versus the quasifission barrier B_{qf} and excitation energy of the compound nucleus, as well as versus the quasifission barrier, B_{qf} and the angular momentum, ℓ are represented in panels (b) and (c), respectively. The red broken (dark) lines corresponding to cut of the complete fusion probability P_{CN}^Z at $E_{\text{CN}}^* = 45$ MeV and at $\ell = 25\hbar$ for each the barrier value B_{qf} are presented in Figs. 5(b) and 5(c).

In order to study the influence of the compound nucleus excitation energy E_{CN}^* and the angular momentum ℓ of the

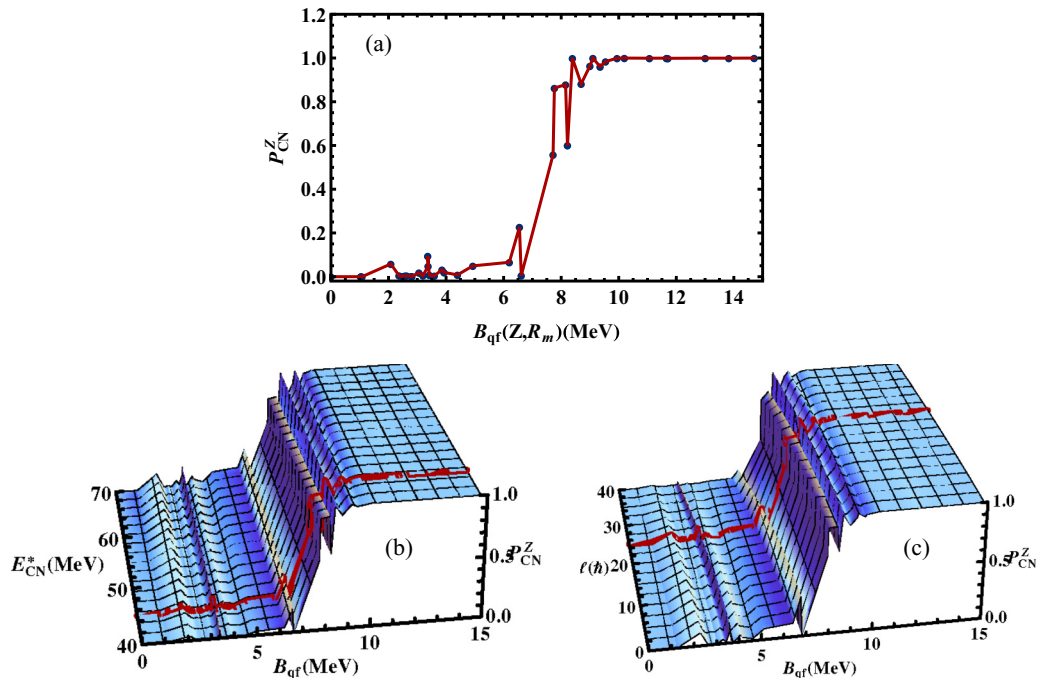


FIG. 5. The calculated probability of complete fusion P_{CN}^Z (dots) for the DNS formed in the reactions leading to the compound nucleus ^{216}Ra as a function of the quasifission barrier B_{qf} at the CN excitation energy $E_{CN}^* = 45$ MeV, and at $\ell = 25\hbar$ in the framework of the DNS model. (a): Obtained results for P_{CN}^Z against B_{qf} and E_{CN}^* in the framework of the DNS model. (b) The complete fusion probability P_{CN}^Z calculated in the DNS model as a function of quasifission barrier B_{qf} and the angular momentum ℓ . (c) The red solid (dark) lines corresponding to cut of P_{CN}^Z at $E_{CN}^* = 45$ MeV and at $\ell = 25\hbar$ for each value B_{qf} are shown in Figs. 6(b) and 6(c), respectively.

interaction system on the complete fusion probability P_{CN}^Z , we studied the variation of P_{CN}^Z in term of E_{CN}^* and ℓ based on the DNS model for the $^{12}\text{C} + ^{204}\text{Pb}$, $^{19}\text{F} + ^{197}\text{Au}$, $^{30}\text{Si} + ^{186}\text{W}$, and $^{48}\text{Ca} + ^{168}\text{Er}$ reactions. In Fig. 6, the results for $\ell = 10\hbar$ and $E_{CN}^* = 50$ MeV are represented as green (light gray) solid, blue large dashed, red dot-dashed, and purple dashed curves (curves from top to bottom) for the $^{12}\text{C} + ^{204}\text{Pb}$, $^{19}\text{F} + ^{197}\text{Au}$, $^{30}\text{Si} + ^{186}\text{W}$, and $^{48}\text{Ca} + ^{168}\text{Er}$ reactions, respectively.

The calculated probability of complete fusion $P_{CN}^Z(Z = 20)$ versus the excitation energy E_{CN}^* for $\ell = 10\hbar$ and $30\hbar$ and for the $^{48}\text{Ca} + ^{168}\text{Er}$ reaction, as brown solid and blue large dashed curves (curves from top to bottom), as well as in terms of

angular momentum ℓ for the excitation energy $E_{CN}^* = 45$ MeV and 50 MeV as purple large dashed and red dashed curves (curves from bottom to top), are shown in Figs. 7(a) and 7(b), respectively. In the case of this system, the fusion barrier B_{fus}^* is high due to the shell effects for the nuclear binding energy in the interval of the charge number Z of the light fragment 30 to 40, the corresponding quasifission barrier is also very small. The complete fusion probability P_{CN}^Z against the excitation energy E_{CN}^* and ℓ for the $^{48}\text{Ca} + ^{168}\text{Er}$ reaction is also plotted in Fig. 7(c). In this figure, the brown solid and blue large dashed curves correspond to cut of P_{CN}^Z at $\ell = 10\hbar$ and $30\hbar$ for a given value E_{CN}^* , and the purple dot-dashed and red dashed curves

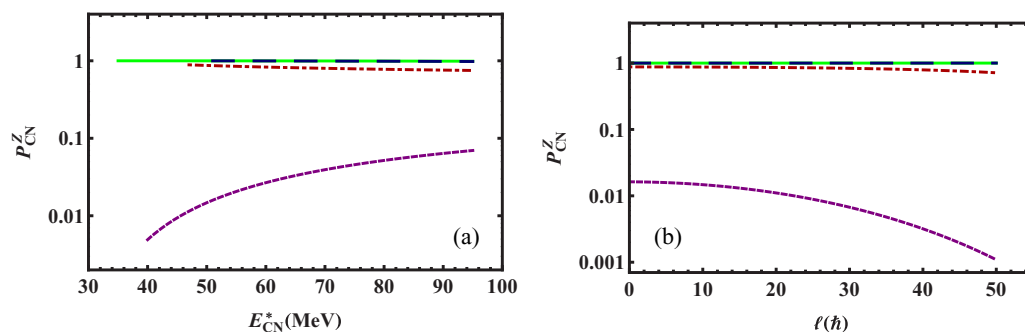


FIG. 6. The calculated probability of complete fusion P_{CN}^Z (dots) for the DNS formed in the reactions leading to the compound nucleus ^{216}Ra as a function of the CN excitation energy E_{CN}^* , and for a given angular momentum $\ell = 10\hbar$ in the framework of the DNS model. (a), and as a function of the angular momentum ℓ and at a given CN excitation energy $E_{CN}^* = 50$ MeV in the framework of the DNS model. (b). The green (light gray) solid, blue large dashed, red dot-dashed, and purple dashed curves (curves from top to bottom) correspond to the $^{12}\text{C} + ^{204}\text{Pb}$, $^{19}\text{F} + ^{197}\text{Au}$, $^{30}\text{Si} + ^{186}\text{W}$, and $^{48}\text{Ca} + ^{168}\text{Er}$ reactions, respectively.

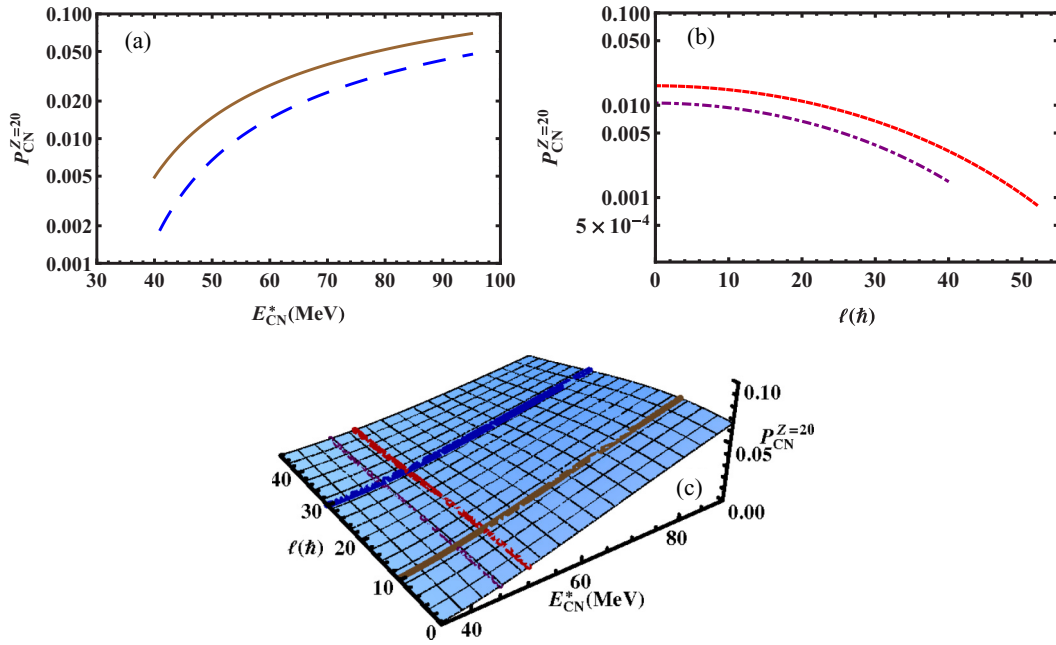


FIG. 7. The calculated probability of complete fusion P_{CN}^Z for the $^{48}\text{Ca} + ^{168}\text{Er}$ reaction as a function of the CN excitation energy E_{CN}^* , in the framework of the DNS model. The brown solid and blue large dashed curves are plotted for $\ell = 10\hbar$ and $30\hbar$ in (a), respectively. The P_{CN}^Z for a given value $Z = 20$ is calculated within the framework of the DNS model as a function of the angular momentum ℓ for a given value of E_{CN}^* . The purple dot-dashed and red dashed curves are plotted for the excitation energies $E_{\text{CN}}^* = 45$ MeV and 50 MeV, respectively, in (b). The complete fusion probability P_{CN}^Z for a given value $Z = 20$ against the excitation energy E_{CN}^* and ℓ for the $^{48}\text{Ca} + ^{168}\text{Er}$ reaction is also plotted in (c).

correspond to a cut of P_{CN}^Z at $E_{\text{CN}}^* = 45$ MeV and 50 MeV for a given value ℓ .

We can stress that in the most symmetric $^{48}\text{Ca} + ^{168}\text{Er}$ reaction, P_{CN}^Z increases with increasing excitation energy E_{CN}^* at given values of ℓ and reduces with increasing ℓ at given values of E_{CN}^* . The complete fusion probability P_{CN}^Z is a function of the barriers of B_{fus}^* and B_{qf} . As a result, taking into account the dependence of these barriers on the angular momentum ℓ , the complete fusion probability decreases with increasing ℓ at given values of the beam energy.

The dependence of the complete fusion probability $P_{\text{CN}}(E_{\text{DNS}}^*, \ell)$ on the CN excitation energy and the angular momentum ℓ is discussed in the framework of the combined

theoretical method based on the DNS approach. It is noted that the complete fusion probability $P_{\text{CN}}(E_{\text{DNS}}^*, \ell)$ is given by a weighted average of the P_{CN}^Z as shown Eq. (21). The obtained results using Eq. (21) for the most symmetric $^{48}\text{Ca} + ^{168}\text{Er}$ reaction are reported in Fig. 8. The brown solid and blue large dashed curves are plotted for $\ell = 10\hbar$ and $30\hbar$, respectively, in panel (a). The purple dot-dashed and red dashed curves are obtained for the excitation energy $E_{\text{CN}}^* = 50$ MeV and 55 MeV, respectively, in panel (b).

The angular momentum and the compound nucleus excitation energy dependence of the complete fusion probability increases with increasing E_{CN}^* , as well as P_{CN} decreases with increasing ℓ as shown in Fig. 8.

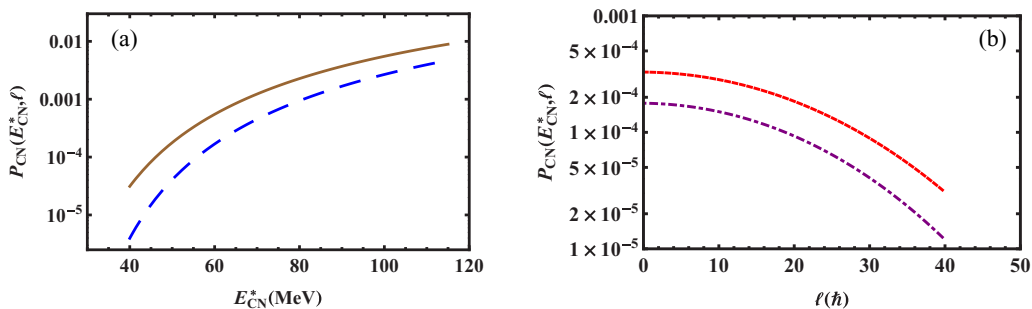


FIG. 8. Calculated complete fusion probability P_{CN} in the framework of DNS concept for the most symmetric $^{48}\text{Ca} + ^{168}\text{Er}$ reaction forming the ^{216}Ra compound nucleus as a function of the E_{CN}^* excitation energy in (a) and of the angular momentum ℓ in (b). The brown solid and blue large dashed curves (curves from top to bottom) in (a) are plotted for $\ell = 10\hbar$ and $30\hbar$, respectively; the purple dot-dashed and red dashed curves (curves from bottom to top) in (b) are plotted for the excitation energy $E_{\text{CN}}^* = 50$ MeV and 55 MeV, respectively.

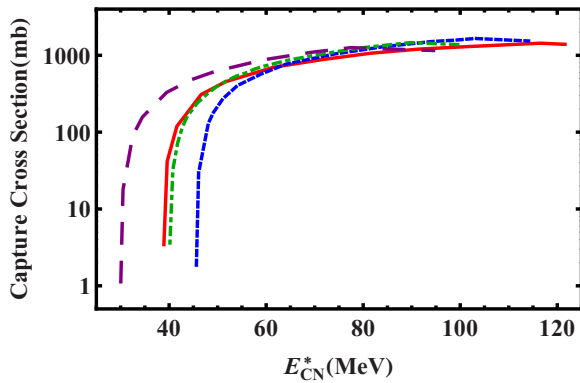


FIG. 9. Capture cross sections predicted within the framework of DNS model for the reactions leading to the formation of the same compound nucleus ^{216}Ra versus the excitation energy E_{CN}^* . The red solid, blue dashed, green dot-dashed, and purple large dashed curves are plotted for the $^{12}\text{C} + ^{204}\text{Pb}$, $^{19}\text{F} + ^{197}\text{Au}$, $^{30}\text{Si} + ^{186}\text{W}$, and $^{48}\text{Ca} + ^{168}\text{Er}$ reactions, respectively.

B. The capture, complete fusion, and quasifission cross section

The heavy ion reaction with the full momentum transfer is called capture reaction. In this stage, the colliding nuclei are trapped into the packet of the nucleus-nucleus potential after the dissipation of part of the initial relative kinetic energy and orbital angular momentum.

To analyze the role of the entrance channel, we compare the results of calculations of the capture, complete fusion, and quasifission cross sections for the $^{12}\text{C} + ^{204}\text{Pb}$, $^{19}\text{F} + ^{197}\text{Au}$, $^{30}\text{Si} + ^{186}\text{W}$, and $^{48}\text{Ca} + ^{168}\text{Er}$ reactions forming the same compound nucleus ^{216}Ra as a function of the CN excitation energy E_{CN}^* within the framework of the DNS model. The results are reported in Figs. 9–11.

Figure 9 shows the difference between the capture cross sections for the four entrance channels with different mass asymmetries. As it is seen, the reaction induced by the lighter projectile has a larger value of the capture cross section than other reactions induced by the heavy projectiles. This strong difference in the capture cross sections is related to the size of the potential pocket in the nucleus-nucleus interaction. For an asymmetry DNS, the interaction potential pocket is deeper and wider than that for a more symmetric configuration corresponding to a given CN.

By comparing the results of Fig. 9 with the ones of Fig. 10 one can observe that in the reactions induced by C and F beams, the fusion cross sections are close to the capture cross sections. Therefore, one can say that for these reactions having higher entrance channel asymmetry, the dominant channel of the DNS evolution is the complete fusion.

The quasifission cross sections predicted for the four reactions, which all lead to the same compound system ^{216}Ra in Fig. 11 indicate that in the case of reactions induced by massive projectiles such as Si and Ca beams, the quasifission process dominates over the fusion process. Hence, for the reactions with lower entrance channel mass asymmetry, the main decay channel is quasifission. Indeed, the $^{12}\text{C} + ^{204}\text{Pb}$, $^{19}\text{F} + ^{197}\text{Au}$, $^{30}\text{Si} + ^{186}\text{W}$, and $^{48}\text{Ca} + ^{168}\text{Er}$ reactions populate the same compound nucleus at similar excitation energies,

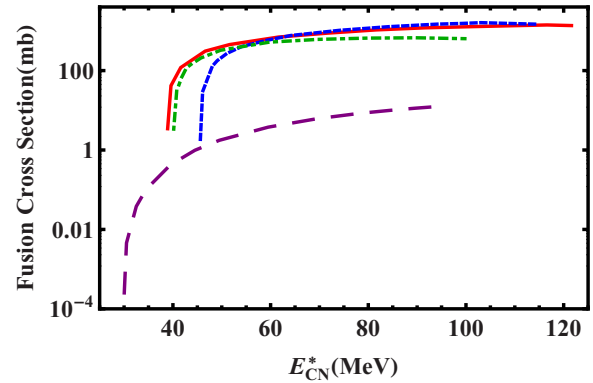


FIG. 10. The fusion cross sections predicted within the framework of the DNS model for the reactions leading to the formation of the same compound nucleus ^{216}Ra versus the excitation energy E_{CN}^* . The red solid, blue dashed, green dot-dashed, and purple large dashed curves are plotted for the $^{12}\text{C} + ^{204}\text{Pb}$, $^{19}\text{F} + ^{197}\text{Au}$, $^{30}\text{Si} + ^{186}\text{W}$, and $^{48}\text{Ca} + ^{168}\text{Er}$ reactions, respectively.

but quasifission signatures observed in the latter two reactions clearly indicate the difference in the dynamical trajectories followed by these systems after capture. The origin of these quasifission events could be related to the entrance channel parameters and the landscape of the potential energy surface associated in heavy ion collision process.

C. Estimation of the relative yields of quasifission and complete fusion processes

The ratios between the quasifission cross section and the capture ones predicted by the DNS model against E_{CN}^* are shown in Fig. 12. The ratios for the four $^{12}\text{C} + ^{204}\text{Pb}$, $^{19}\text{F} + ^{197}\text{Au}$, $^{30}\text{Si} + ^{186}\text{W}$, and $^{48}\text{Ca} + ^{168}\text{Er}$ reactions are shown as the red solid, blue dashed, green dot-dashed, and purple large dashed curves in panels (a) and (b), respectively. It

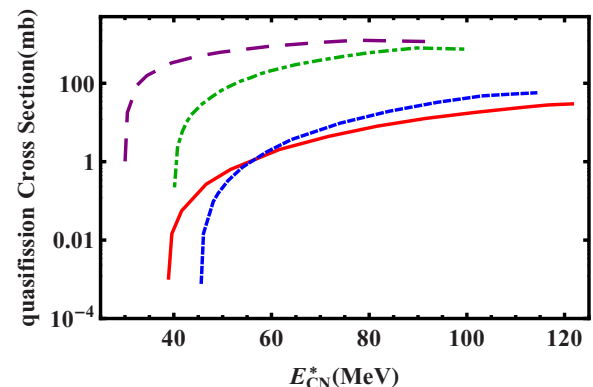


FIG. 11. The prediction of quasifission cross sections in the framework of the DNS model for the reactions leading to the formation of the same compound nucleus ^{216}Ra versus the excitation energy E_{CN}^* . The red solid, blue dashed, green dot-dashed, and purple large dashed curves (curves from bottom to top) are plotted for the $^{12}\text{C} + ^{204}\text{Pb}$, $^{19}\text{F} + ^{197}\text{Au}$, $^{30}\text{Si} + ^{186}\text{W}$, and $^{48}\text{Ca} + ^{168}\text{Er}$ reactions, respectively.

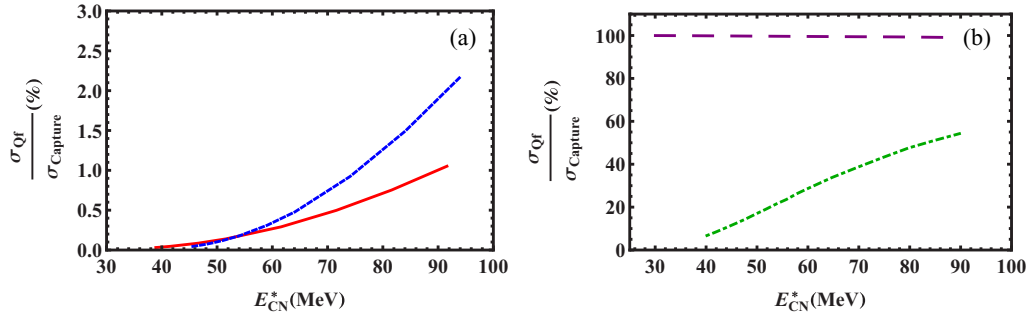


FIG. 12. The prediction of quasifission probability in the framework of the DNS model for the four entrance channels with different mass asymmetries leading to the same compound nucleus ^{216}Ra versus the excitation energy E_{CN}^* . The red solid and blue dashed curves (curves from bottom to top) reported in (a) are related to the $^{12}\text{C} + ^{204}\text{Pb}$ and $^{19}\text{F} + ^{197}\text{Au}$ reactions, respectively; the green dot-dashed, and purple large dashed curves (curves from bottom to top) reported in (b) are related to the $^{30}\text{Si} + ^{186}\text{W}$ and $^{48}\text{Ca} + ^{168}\text{Er}$ reactions, respectively.

is seen that the contribution of quasifission component is only around between 0 to 1% for the $^{12}\text{C} + ^{204}\text{Pb}$ reaction system and 0 to 2% for the $^{19}\text{F} + ^{197}\text{Au}$ reaction system at excitation energy interval 40 MeV and 90 MeV. Therefore, the model predicts a negligible quasifission probability for the $^{12}\text{C} + ^{204}\text{Pb}$ and $^{19}\text{F} + ^{197}\text{Au}$ reactions, in agreement with the experimental results [10,33]. Whereas, an approximately 5 to 55% contribution of quasifission signature have been predicted for the $^{30}\text{Si} + ^{186}\text{W}$ reaction system in the energy range studied in this work. A large contribution of the quasifission rate is manifested for the most symmetric $^{48}\text{Ca} + ^{168}\text{Er}$ reaction.

Since the capture cross section in the DNS model is equal to the sum of complete fusion and quasifission cross sections, $\sigma_{\text{cap}} = \sigma_{\text{fus}} + \sigma_{\text{qf}}$, the probability of complete fusion can be defined by the ratio of the complete fusion and capture cross sections, $P_{\text{CN}} = (1 - \sigma_{\text{qf}}/\sigma_{\text{cap}}) \times 100$. Figure 13 shows the behavior of the fusion probability P_{CN} as a function of E_{CN}^* for a given value $Z = 20$. The ratios of the fusion and capture cross sections for the $^{12}\text{C} + ^{204}\text{Pb}$ and $^{19}\text{F} + ^{197}\text{Au}$; $^{30}\text{Si} + ^{186}\text{W}$ and $^{48}\text{Ca} + ^{168}\text{Er}$ reactions can be due to the formation of the ^{216}Ra element are indicated in Figs. 13(a) and 13(b), respectively. It should be mentioned that the fusion probability for the $^{48}\text{Ca} + ^{168}\text{Er}$ reaction is multiplied by a factor 30, since this quantity is very small for this reaction. The analysis of

the details of calculations of P_{CN} for the above mentioned reactions shows that the behavior of P_{CN} is different for the charge asymmetric and symmetric reactions. The inner fusion barriers B_{fus}^* for the $^{30}\text{Si} + ^{186}\text{W}$ and $^{48}\text{Ca} + ^{168}\text{Er}$ reactions are larger than those for the $^{12}\text{C} + ^{204}\text{Pb}$, $^{19}\text{F} + ^{197}\text{Au}$ reactions. As one can see, P_{CN} is about 100% for the $^{12}\text{C} + ^{204}\text{Pb}$ reaction (very mass asymmetric reaction) that its value slightly reduces in higher quantities of excitation energy E_{CN}^* . Therefore, the DNS formed in this reaction evolves almost fully to the compound nucleus. In the case of the most symmetric $^{48}\text{Ca} + ^{168}\text{Er}$ reaction, the quasifission channel is dominant in the evolution of DNS, and the fusion process is extremely hindered.

IV. CONCLUSIONS

The theoretical method based on the dinuclear system approach is utilized to investigate the influence of entrance channel mass (charge) asymmetry on the process of compound nucleus formation. The $^{12}\text{C} + ^{204}\text{Pb}$, $^{19}\text{F} + ^{197}\text{Au}$, $^{30}\text{Si} + ^{186}\text{W}$, and $^{48}\text{Ca} + ^{168}\text{Er}$ reactions which all lead to the compound nucleus ^{216}Ra at similar excitation energies are discussed. The emission barriers of inner fusion B_{fus}^* and quasifission B_{qf} , as well as capture, complete fusion, and quasifission cross sections in the reactions with massive nuclei are calculated

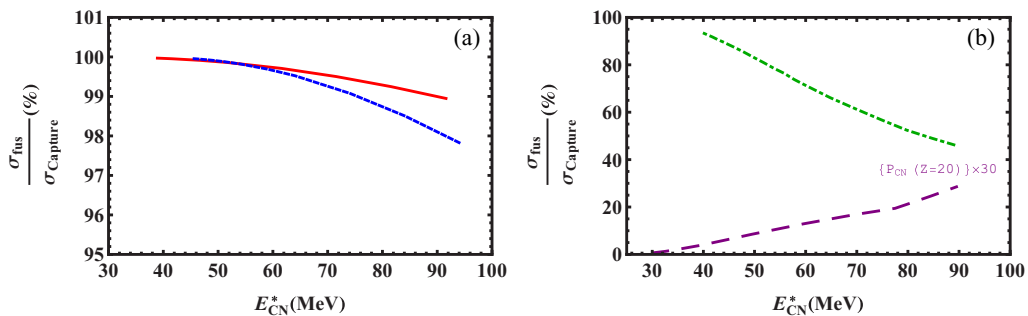


FIG. 13. The fusion probability $P_{\text{CN}} = \sigma_{\text{fus}}/\sigma_{\text{cap}} \times 100$ calculated for the different reactions formed the same compound nucleus ^{216}Ra as a function of the CN excitation energy. The red solid and blue dashed curves (curves from top to bottom) reported in (a) are related to the $^{12}\text{C} + ^{204}\text{Pb}$ and $^{19}\text{F} + ^{197}\text{Au}$ reactions, respectively; the green dot-dashed, and purple large dashed curves (curves from top to bottom) reported in (b) are related to the $^{30}\text{Si} + ^{186}\text{W}$ and $^{48}\text{Ca} + ^{168}\text{Er}$ reactions, respectively.

by using the double-folding formation for the nuclear part of internuclear potential at pole-pole orientation.

The competition between complete fusion and quasifission channels is considered by means of the calculation of complete fusion probability P_{CN}^Z . We can stress that this probability strongly depends on the mass asymmetry of entrance channel, excitation energy of the dinuclear system E_{DNS}^* , and angular momentum ℓ . The calculations show that in the systems with high asymmetry of colliding nuclei and having a deep interaction potential pocket, P_{CN}^Z increases with increasing the excitation energy E_{CN}^* at given values of ℓ and reduces with increasing ℓ at given values of E_{CN}^* . The complete fusion probability P_{CN}^Z is a function of the barriers of B_{fus}^* and B_{qf} . Hence, taking into account the dependence of these barriers on ℓ , the probability P_{CN}^Z decreases with increasing ℓ at given values of the beam energy. It is already shown that the barriers B_{qf} and B_{fus}^* play crucial roles in complete fusion, and depend on the DNS charge asymmetry and angular momentum of the DNS. Indeed, reactions with a small B_{fus}^* and a large B_{qf} are favorable for the complete fusion.

The analysis of theoretical results indicates that among reactions leading to the same composite system, the reaction induced by the lighter projectile has a larger value of the capture cross section than other reactions induced by the heavy projectiles. This strong difference in the capture cross sections is connected to the size of the potential pocket in the nucleus-nucleus interaction. For an asymmetry DNS, the interaction potential pocket is deeper and wider than that for a more symmetric configuration corresponding to a given CN.

The DNS model calculations have been also performed to estimate the relative yield of quasifission in the $^{12}\text{C} + ^{204}\text{Pb}$, $^{19}\text{F} + ^{197}\text{Au}$, $^{30}\text{Si} + ^{186}\text{W}$, and $^{48}\text{Ca} + ^{168}\text{Er}$ reactions. It is seen that the contributions of the quasifission component in the $^{12}\text{C} + ^{204}\text{Pb}$ and $^{19}\text{F} + ^{197}\text{Au}$ reaction systems are only around between 0 to 1% and 0 to 2% at excitation energy interval 40 MeV and 90 MeV, respectively. Therefore, the model predicts a negligible quasifission probability for these reactions having higher entrance channel mass symmetry and the dominant decay channel is complete fusion.

For the $^{30}\text{Si} + ^{186}\text{W}$ reaction system we have been predicted an approximately 5 to 55% contribution of quasifission signature in the energy range studied in this work. A large contribution of quasifission components is manifested for the most symmetric combination $^{48}\text{Ca} + ^{168}\text{Er}$ reaction on the whole range of excitation energy E_{CN}^* . Therefore, one can say that in the case of reactions induced by massive projectiles such as Si and Ca having lower entrance channel mass asymmetry, the quasifission component is dominant in the evolution of the DNS, and the fusion process is extremely hindered.

It should be emphasized that although the $^{12}\text{C} + ^{204}\text{Pb}$, $^{19}\text{F} + ^{197}\text{Au}$, $^{30}\text{Si} + ^{186}\text{W}$, and $^{48}\text{Ca} + ^{168}\text{Er}$ reactions leading to the same composite system ^{216}Ra , quasifission signatures observed in the latter two reactions clearly indicate the difference in the dynamical trajectories followed by these systems after capture. The origin of these quasifission events could be related to the entrance channel parameters and the landscape of the potential energy surface associated with the massive nuclei collision process.

-
- [1] W. J. Swiatecki, *Phys. Scr.* **24**, 113 (1981).
- [2] J. P. Blocki, H. Feldmeier, and W. J. Swiatecki, *Nucl. Phys. A* **459**, 145 (1986).
- [3] B. B. Back, P. B. Fernandez, B. G. Glagola, D. Henderson, S. Kaufman, J. G. Keller, S. J. Sanders, F. Videbaek, T. F. Wang, and B. D. Wilkins, *Phys. Rev. C* **53**, 1734 (1996).
- [4] D. J. Hinde, M. Dasgupta, J. R. Leigh, J. P. Lestone, J. C. Mein, C. R. Morton, J. O. Newton, and H. Timmers, *Phys. Rev. Lett.* **74**, 1295 (1995).
- [5] D. J. Hinde, M. Dasgupta, J. R. Leigh, J. C. Mein, C. R. Morton, J. O. Newton, and H. Timmers, *Phys. Rev. C* **53**, 1290 (1996).
- [6] G. Fazio, G. Giardina, F. Hanappe, G. Mandaglio, M. Manganaro, A. I. Muminov, A. K. Nasirov, and C. Saccà, *J. Phys. Soc. Jpn.* **77**, 124201 (2008).
- [7] A. K. Nasirov, A. I. Muminov, R. K. Utamuratov, G. Fazio, G. Giardina, F. Hanappe, G. Mandaglio, M. Manganaro, and W. Scheid, *Eur. Phys. J. A* **34**, 325 (2007).
- [8] C. J. Lin, R. du Rietz, D. J. Hinde, M. Dasgupta, R. G. Thomas, M. L. Brown, M. Evers, L. R. Gasques, and M. D. Rodriguez, *Phys. Rev. C* **85**, 014611 (2012).
- [9] R. du Rietz, E. Williams, D. J. Hinde, M. Dasgupta, M. Evers, C. J. Lin, D. H. Luong, C. Simenel, and A. Wakhle, *Phys. Rev. C* **88**, 054618 (2013).
- [10] A. Yu. Chizhov, M. G. Itkis, I. M. Itkis, G. N. Kniajeva, E. M. Kozulin, N. A. Kondratiev, I. V. Pokrovsky, R. N. Sagaidak, V. M. Voskressensky, A. V. Yerebin, L. Corradi, A. Gadea, A. Latina, A. M. Stefanini, S. Szilner, M. Trotta, A. M. Vinodkumar, S. Beghini, G. Montagnoli, F. Scarlassara, A. Ya. Rusanov, F. Hanappe, O. Dorvaux, N. Rowley, and L. Stuttge, *Phys. Rev. C* **67**, 011603(R) (2003).
- [11] A. Wakhle, C. Simenel, D. J. Hinde, M. Dasgupta, M. Evers, D. H. Luong, R. du Rietz, and E. Williams, *Phys. Rev. Lett.* **113**, 182502 (2014).
- [12] G. Fazio, G. Giardina, G. Mandaglio, F. Hanappe, A. I. Muminov, A. K. Nasirov, W. Scheid, and L. Stuttgé, *Mod. Phys. Lett. A* **20**, 391 (2005).
- [13] E. A. Cherepanov, *PRAMANA J. Phys.* **53**, 619 (1999).
- [14] G. Giardina, F. Hanappe, A. I. Muminov, A. K. Nasirov, and L. Stuttge, *Nucl. Phys. A* **671**, 165 (2000).
- [15] H. Q. Zhang, C. L. Zhang, C. J. Lin, Z. H. Liu, F. Yang, A. K. Nasirov, G. Mandaglio, M. Manganaro, and G. Giardina, *Phys. Rev. C* **81**, 034611 (2010).
- [16] Q. Li, W. Zuo, W. Li, N. Wang, E. Zhao, J. Li, and W. Scheid, *Eur. Phys. J. A* **24**, 223 (2005).
- [17] G. Mandaglio, G. Fazio, G. Giardina, F. Hanappe, M. Manganaro, A. I. Muminov, A. K. Nasirov, and C. Saccà, *Phys. At. Nucl.* **72**, 1639 (2009).
- [18] A. Nasirov, A. Fukushima, Y. Toyoshima, Y. Aritomo, A. Muminov, Sh. Kalandarov, and R. Utamuratov, *Nucl. Phys. A* **759**, 342 (2005).
- [19] P. Papka and C. Beck, *Lecture Notes in Physics* (Springer, Berlin, 2012), Vol. 848, p. 299.
- [20] G. Audi, A. H. Wapstra, and C. Thibault, *Nucl. Phys. A* **729**, 337 (2003).
- [21] P. Moller, J. R. Nix, W. D. Myers, and W. J. Swiatecki, *At. Data Nucl. Data Tables* **59**, 185 (1995).

- [22] C. Y. Wong, *Phys. Rev. Lett.* **31**, 766 (1973).
- [23] G. G. Adamian, N. V. Antonenko, R. V. Jolos, S. P. Ivanova, and O. I. Melnikova, *IJMPE* **5**, 191 (1996).
- [24] G. G. Adamian, N. V. Antonenko, and Sh. A. Kalandarov, *Phys. Part. Nucl.* **47**, 1 (2016).
- [25] Sh. A. Kalandarov, G. G. Adamian, N. V. Antonenko, and W. Scheid, *Phys. Rev. C* **82**, 044603 (2010).
- [26] G. G. Adamian, N. V. Antonenko, and A. S. Zubov, *Phys. Part. Nucl.* **45**, 848 (2014).
- [27] G. G. Adamian, N. V. Antonenko, and W. Scheid, *Phys. Rev. C* **68**, 034601 (2003).
- [28] G. Fazio, G. Giardina, A. Lamberto, C. Saccà, R. Palamara, A. I. Muminov, A. K. Nasirov, K. V. Pavliy, F. Hanappe, T. Materna, and L. Stuttgé, *J. Phys. Soc. Jpn.* **74**, 307 (2005).
- [29] G. Fazio, G. Giardina, A. Lamberto, R. Ruggeri, C. Saccà, R. Palamara, A. I. Muminov, A. K. Nasirov, U. T. Yakhshiev, F. Hanappe, T. Materna, and L. Stuttgé, *J. Phys. Soc. Jpn.* **72**, 2509 (2003).
- [30] G. Fazio, G. Giardina, A. Lamberto, R. Ruggeri, C. Saccà, R. Palamara, A. I. Muminov, A. K. Nasirov, U. T. Yakhshiev, F. Hanappe, T. Materna, and L. Stuttgé, *Eur. Phys. J. A* **19**, 89 (2004).
- [31] S. Giardina, A. I. Hofmann, Muminov, and A. K. Nasirov, *Eur. Phys. J. A* **8**, 205 (2000).
- [32] W. Scobel, H. H. Gutbrod, M. Blann, and A. Mignerey, *Phys. Rev. C* **14**, 1808 (1976).
- [33] R. N. Sagaidak, G. N. Kniajeva, I. M. Itkis, M. G. Itkis, N. A. Kondratiev, E. M. Kozulin, I. V. Pokrovsky, A. I. Svirikhin, V. M. Voskressensky, A. V. Yerebin, L. Corradi, A. Gadea, A. Latina, A. M. Stefanini, S. Szilner, M. Trotta, A. M. Vinodkumar, S. Beghini, G. Montagnoli, F. Scarlassara, D. Ackermann, F. Hanappe, N. Rowley, and L. Stuttge, *Phys. Rev. C* **68**, 014603 (2003).